Optical Engineering

OpticalEngineering.SPIEDigitalLibrary.org

Moiré effect in displays: a tutorial

Vladimir Saveljev
Sung-Kyu Kim
Jaisoon Kim

SPIE.

Vladimir Saveljev, Sung-Kyu Kim, Jaisoon Kim, "Moiré effect in displays: a tutorial," *Opt. Eng.* **57**(3), 030803 (2018), doi: 10.1117/1.OE.57.3.030803.

Optical Engineering 57(3), 030803 (March 2018)

TUTORIAL

Moiré effect in displays: a tutorial

Vladimir Saveljev,[a,*] Sung-Kyu Kim,[b] and Jaisoon Kim[a]
[a]Myongji University, Department of Physics, Yongin, Gyeonggi-do, Republic of Korea
[b]Korea Institute of Science and Technology (KIST), Center for Image Media Research, Seongbuk-gu, Seoul, Republic of Korea

Abstract. The tutorial describes essential features of moiré patterns, as well as the circumstances, when the moiré patterns appear and how to estimate their characteristics (parameters) such as the orientation and period. The moiré effect is described in two domains, the image space (spatial domain) and in the spectral domain using the complex numbers. The tutorial covers the indicial equation method, the coplanar and non-coplanar sinusoidal gratings, the moiré effect in a spatial object (a cylinder), as well as explains the moiré wave vector, the moiré spectra, the spectral trajectories, and summarizes behavior of the visible patterns in moved/rotated gratings. [DOI: 10.1117/1.OE.57.3.030803]

Keywords: moiré effect; moiré minimization; moiré patterns; spectral trajectories; cylindrical moiré; autostereoscopic displays.

Paper 171942T received Dec. 5, 2017; accepted for publication Mar. 2, 2018; published online Mar. 28, 2018; corrected Sep. 13, 2018.

1 Introduction

The moiré effect is a physical phenomenon of linear optics. The moiré patterns appear as a result of an interaction between transparent layers of a repeated structure[1] when superposed layers are viewed through. Several examples of the moiré effect are shown in Fig. 1 (a bridge, a facade of a building, an air conditioner grid, a textile curtain, etc.).

The visual appearance of the moiré patterns depends on characteristics of gratings and on the location of the observer.[2] In the case of two gratings, the patterns look like an added series of repeated stripes, which could look bright, vivid, and sometimes even unpredictable.

The moiré effect is not unknown in the literature. A general description of the moiré effect can be found in several books (Refs. 1–3), which also include many useful examples. A perfectly illustrated book, Ref. 4 is full of excellent moiré images. There are also research papers, specifically Refs. 5–10, which describe various aspects of the moiré effect. Examples of the moiré effect in digital devices are shown in Fig. 2.

In gratings of similar layouts, the moiré patterns reproduce the structure of the gratings as in the moiré magnifier,[11] see Fig. 3. This figure also shows that with all other conditions equal, the period of the moiré patterns is the same in gratings of different geometric layouts.

Generally speaking, visual displays can be either dynamic or static. The dynamic displays are CRT TV, LCD, and OLED. The examples of static displays are a printed picture or photograph, poster, and postcard. In visual displays, the moiré effect may create an unwanted and sometimes unexpected image of bands (as in Fig. 1) or patterns (as in Fig. 3). Such additional visual background decreases the contrast on the display screen and consequently reduces the image quality; therefore in imaging and displays, the moiré effect is an undesirable adverse visual effect.[12,13] The elimination or the reduction of the moiré patterns in displays is an important issue of improvement in the visual quality. The necessity of the minimization of the moiré patterns in three-dimensional (3-D) displays was first stated[14] in the early 2000s. This is especially important for autostereoscopic 3-D displays,[15–23] where the moiré effect may often occur due to their typical design.

The moiré effect was observed not only under visible light but also under rays and beams of different nature, for instance, in electron beams,[23] infrared light,[24] and x-rays,[25] as well as at the nanoscale in graphene layers.[26]

Finding characteristics of patterns based on the layouts of the layers is a direct problem.[27–31] An inverse problem is to find the position (shape) of another grating based on the observed moiré patterns when positions of an observer and of one grating are known together with the parameters of the grating; this is a topic of the 3-D shape measurement.[2,32–37]

In contrast, it appears to be possible to arrange the moiré patterns so the resulting pattern would carry useful informational content (including 3-D). The first solution of this previously unknown moiré problem was proposed in Ref. 38 and implemented in Ref. 39. Also, the moiré effect can be used for other purposes, such as the moiré interferometry,[40–42] the moiré deflectometry,[43] the optical alignment,[44,45] the visual security (cryptography),[46,47] and many other applications.

That is to say, this is a twofold moiré problem that on the one hand, deals with minimization of the moiré effect to improve the image quality;[48] and on the other hand, with its maximization to measure distances,[49,50] as well as to display meaningful images[38] in 3-D displays based entirely on the moiré effect as the main physical principle, or to improve security.[51–53] An image in a 3-D moiré display is shown in Fig. 4. In each application example mentioned in this paragraph, the understanding of the behavior of the moiré patterns is needed.

There are many approaches to investigate the moiré effect. In some cases, solutions can be found from direct analytical considerations. The indicial method can be used to find locations of the characteristic points (minima or maxima) of the patterns. The indicial and direct approaches require simplification, such as a simplified structure, small angles, smooth functions (nearly sinusoidal), etc.

*Address all correspondence to: Vladimir Saveljev, E-mail: saveljev.vv@gmail.com

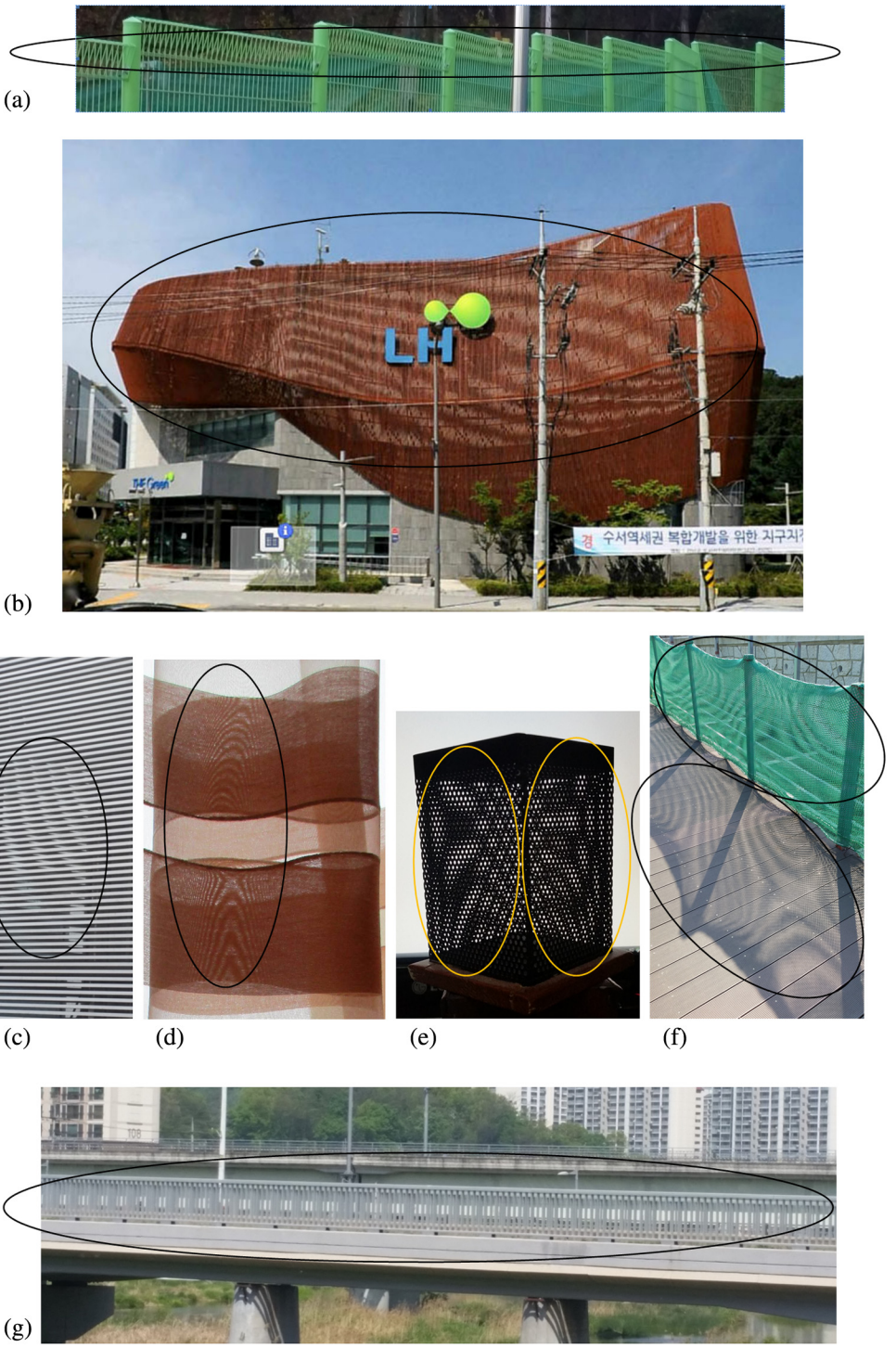

Fig. 1 Moiré patterns around us (a) fence, (b) building, (c) air conditioner grid of a building (d) curtain, (e) pen holder, (f) mesh and its shadow, and (g) bridge.

Dealing with spectra represents a generalized approach.[54–56] Using spectral trajectories,[57] the behavior of the patterns can be estimated geometrically. As the equations of the trajectories are derived from the geometric characteristics of the gratings, the estimation can be made without calculations of spectra. This makes the spectral trajectories suitable for an interactive computer simulation.

The tutorial is based on the authors' knowledge and comprehension of the moiré phenomenon and experience in investigating it for a decade. It includes several methods to find characteristics of the moiré patterns in various situations that are presented.

After sections, we provide exercises. We hope that the exercises can make readers to think deeply, and this way to improve their understanding of the considered topics. Implied is a self-check as, for example, the same result obtained by an independent method. This is probably one of the best methods of verification. Nevertheless, whenever

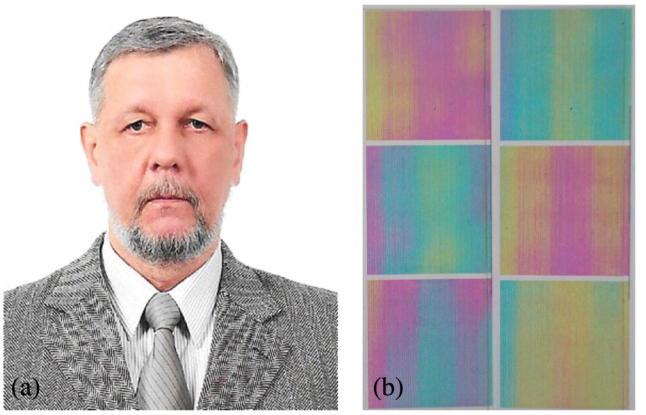

Fig. 2 Moiré patterns in the digital world (a) scanned image and (b) 3-D displays.

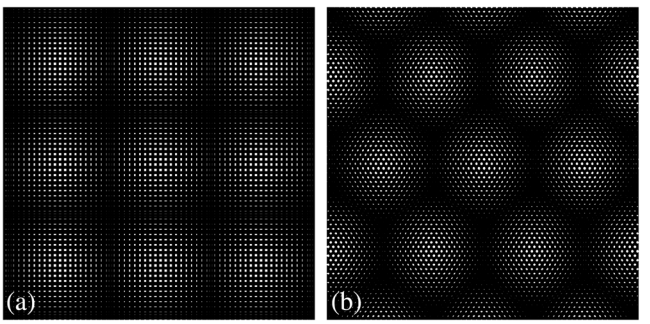

Fig. 3 Same period of moiré patterns in (a) square and (b) hexagonal grids of identical periods.

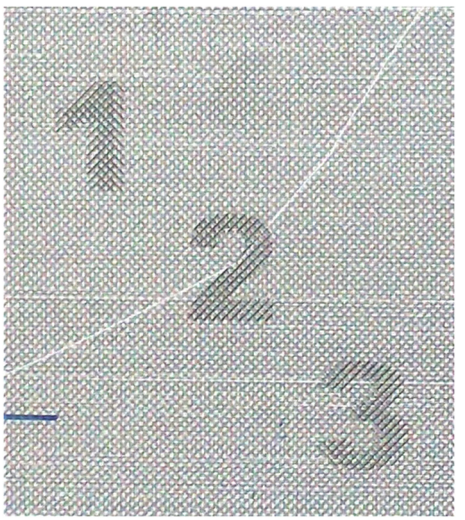

Fig. 4 Image in a moiré display.

readers would send their solutions to the authors, the readers' notes and comments will be considered and replied to with the greatest pleasure.

The tutorial is arranged as follows: Secs. 2–5 deal with the moiré effect directly, in the spatial domain, whereas Secs. 6–8 deal with spectra (the spectral domain). Namely, in Sec. 2, we explain the indicial equation method. In Secs. 3 and 4, we describe the plain coplanar and noncoplanar sinusoidal gratings. Section 5 gives an example of the moiré effect in a 3-D object, a cylinder. Then, Secs. 6 and 7 present such fundamental issues as the wave vector of the moiré patterns in terms of the vector sum and the basics of two-dimensional (2-D) Fourier transform. Section 8 describes the spectral trajectories. After discussion about the visual effects in displaced or rotated plane gratings in Sec. 9, a conclusion finalizes the tutorial.

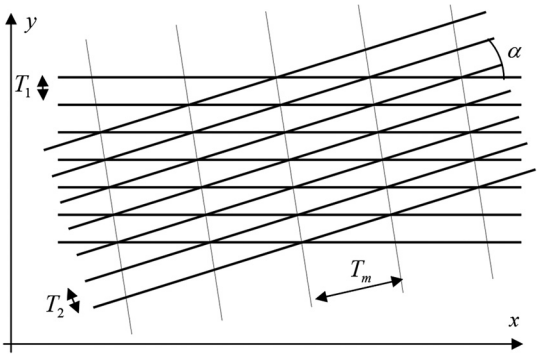

Fig. 5 Sketch of the indices.

2 Indicial Equation

The indicial equation is an analytical method to calculate the characteristic locations of fringes, implying that the locations of the minima/maxima of gratings are known. In this approach, a line grating is modeled by a series of thin lines (a sketch of a family of lines), i.e., some kind of a wire-frame of the maxima (or minima) only, with the intensity profile ignored. The lines of the moiré bands connect the intersections of these families of lines of gratings. As soon as the equations of these intersections can be calculated based on the given equations of the families, technically the equations of the moiré bands can be found as analytical expressions.

As an easy example, consider two families of the equidistant parallel lines in the xy-plane: the horizontal lines with period T_1 and the slanted lines with period T_2 (rotated at the angle α). The sketch lines of the gratings are shown by solid lines in Fig. 5; the moiré patterns comprise the third family of lines with the period T_m at the angle θ (shown by dotted lines connecting the intersections in a shortest way). These spots or relatively low visual densities are visually connected as brighter spaces between darker areas, and the moiré patterns appear.

The periods of bright and dark lines are identical. Without loss of generality, consider the maxima. The equations of two families are

$$y = mT_1, \tag{1}$$

$$x \sin \alpha + y \cos \alpha = nT_2, \tag{2}$$

where x, y are coordinates, m and n are the integer numbers enumerating the lines in the families. The p'th line connects the intersections with the following numbers:

$$m - n = q, \tag{3}$$

where q is another integer.

Excluding m and n from Eqs. (1)–(3), we obtain the equation of the q'th intersection, i.e., the q'th moiré line

$$-xT_1 \sin\alpha + y(T_2 - T_1\cos\alpha) = T_1T_2q. \tag{4}$$

This equation represents the family of the parallel lines of lower spatial frequency (whose period is longer than the period of either grating). From the equation of the straight line, Eq. (4) can be rewritten in the normal form

$$y\sin\theta + x\cos\theta - p = 0. \tag{5}$$

We can obtain the tangent of the orientation angle of the moiré line

$$\tan\theta = \frac{-T_1\sin\alpha}{T_2 - T_1\cos\alpha} = \frac{-\sin\alpha}{\frac{T_2}{T_1} - \cos\alpha}, \tag{6}$$

as well as the distance between two successive moiré lines (when the index q changes by one unit), i.e., the period of the moiré patterns

$$T_m = \frac{T_1T_2}{\sqrt{T_1^2 - 2T_1T_2\cos\alpha + T_2^2}} = \frac{T_2}{\sqrt{1 - 2\frac{T_2}{T_1}\cos\alpha + \left(\frac{T_2}{T_1}\right)^2}}. \tag{7}$$

In the case of the identical gratings ($T_1 = T_2$), Eqs. (6) and (7) are simplified. The angle becomes

$$\tan\theta = \frac{-\sin\alpha}{1 - \cos\alpha} = -\cot\frac{\alpha}{2}, \tag{8}$$

which means the half angle between the gratings of equal periods; the period in this case is

$$T_m = \frac{T_1}{2\sin\frac{\alpha}{2}}. \tag{9}$$

Equations (6) and (7) correspond to Eq. (2.9) from Ref. 1 with $\theta_1 = 0$, whereas Eqs. (8) and (9) correspond to Eq. (2.10) there. A visual illustration of the moiré effect in the identical gratings is shown in Fig. 6 ($\alpha = 5$ deg).

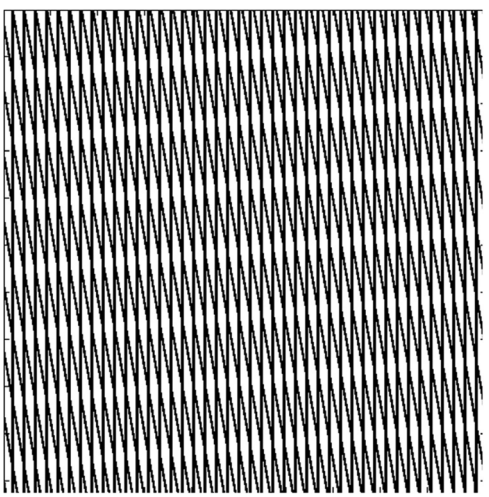

Fig. 6 Moiré patterns in overlapped gratings.

2.1 *Exercises*

1. Calculate the period and orientation of the moiré patterns in the parallel line gratings with their periods 1 and 1.1 mm.
2. The same for the identical gratings (period 2 mm) installed at the angles of 0 deg, 5 deg, and 10 deg.
3. Calculate the period of the moiré patterns in the square grids with the same periods and angles as in the problems 1 and 2.
4. The same for the line grating 1 mm and 30 deg-rhomboidal grid 1.1 mm at the angle of 25 deg between them.
5. Describe the shape of the moiré patterns in the circular (radial/concentric) grating + line grating.

3 Sinusoidal Coplanar Gratings

The profile of the gratings also can be taken into account. For example, the analytical expressions of the moiré bands can be obtained for the sinusoidal gratings. The moiré patterns are the patterns of a longer period. The estimation of their visual appearance is based on the wave numbers.

3.1 *Two Line Gratings*

An interaction between the gratings can be modeled mathematically by the multiplication of transparency functions of the gratings. For instance, a one-dimensional (1-D) sinusoidal line grating (whose intensity profile along certain direction is a sinusoidal function) can be described by its transparency function $t = (1 + \cos\mathbf{k}\cdot\mathbf{x})/2$, where $\mathbf{k}$ is the wave vector (inversely proportional to the period), and $\mathbf{x}$ is the coordinate axis. A sinusoidal grating is shown in Fig. 7(a).

A result of the interaction between two gratings Fig. 7(a) can be written as

$$\begin{aligned} t_{12} = t_1t_2 &= \frac{1}{2}[1 + \cos(\mathbf{k}_1\cdot\mathbf{x})]\cdot\frac{1}{2}[1 + \cos(\mathbf{k}_2\cdot\mathbf{x})] \\ &= \frac{1}{4}[1 + \cos(\mathbf{k}_1\cdot\mathbf{x}) + \cos(\mathbf{k}_2\cdot\mathbf{x}) + \cos(\mathbf{k}_1\cdot\mathbf{x})\cos(\mathbf{k}_2\cdot\mathbf{x})] \\ &= \frac{1}{4}\left\{1 + \cos(\mathbf{k}_1\cdot\mathbf{x}) + \cos(\mathbf{k}_2\cdot\mathbf{x}) + \frac{1}{2}\cos[(\mathbf{k}_1 + \mathbf{k}_2)\cdot\mathbf{x}]\right. \\ &\quad \left. + \frac{1}{2}\cos[(\mathbf{k}_1 - \mathbf{k}_2)\cdot\mathbf{x}]\right\}, \end{aligned} \tag{10}$$

where $\mathbf{k}_1$ and $\mathbf{k}_2$ are the wave vectors of the gratings; the expression $\mathbf{k}\cdot\mathbf{x}$ means the dot product of the vectors $\mathbf{k}$ and $\mathbf{x}$.

For the moiré effect, we need the smallest wave number. In Eq. (10), the first term is the constant bias (a "DC" term), the second and third terms are the gratings themselves, whereas the fourth and fifth terms represent combinational spatial frequencies (sum and difference). In Eq. (10), the term with the smallest wave number (and with the lowest spatial frequency) is the fourth term proportional to $\cos[(\mathbf{k}_1 - \mathbf{k}_2)\cdot\mathbf{x}]$.

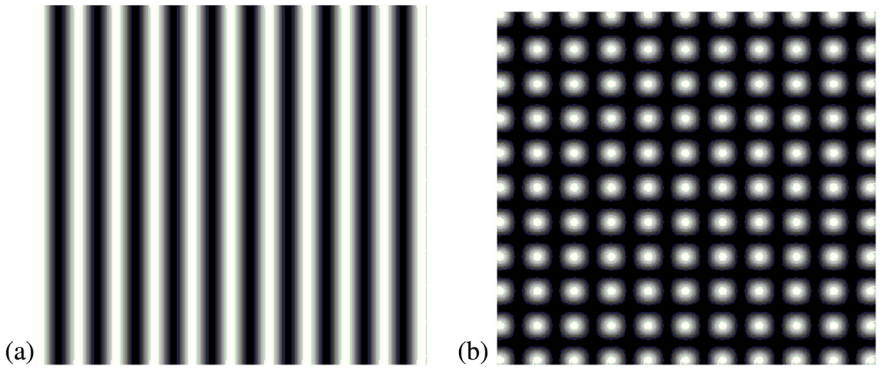

Fig. 7 (a) Sinusoidal 1-D grating and (b) sinusoidal 2-D grid.

3.2 *Square Grid + Line Grating*

Superimposed gratings model a typical structure of many displays. A square grid can be thought as a pair of overlapped orthogonal gratings, whereas the barrier (or lenticular) plate can be modeled by a line grating. Accordingly, for two superposed rectangular gratings, we need two such pairs, four gratings total. For the square grid superposed with the line grating, we need three gratings. Examples of the grating and the grid are shown in Fig. 7.

The transparency function of overlapped gratings obtained by the multiplication is

$$t_{123} = t_1 t_2 t_3 = \frac{1}{16}[1 + \cos(\mathbf{k}_{1x} \cdot \mathbf{x}_1)][1 + \cos(\mathbf{k}_{1y} \cdot \mathbf{y}_1)] \times [1 + \cos(\mathbf{k}_{2x} \cdot \mathbf{x}_2)]. \tag{11}$$

The vector relationship Eq. (11) can be rewritten in a scalar form. For that purpose, the dot products in Eq. (11) can be rewritten as follows:

$$\begin{aligned} \mathbf{k}_{1x} \cdot \mathbf{x}_1 &= \rho k(1,0) \cdot (x, y) = \rho k x \\ \mathbf{k}_{1y} \cdot \mathbf{y}_1 &= \rho k(0,1) \cdot (x, y) = \rho k y \\ \mathbf{k}_{2x} \cdot \mathbf{x}_2 &= k(\cos\alpha, \sin\alpha) \cdot (x, y) \\ &= k(x\cos\alpha + y\sin\alpha), \end{aligned} \tag{12}$$

where k is the wave number of the first grating, α is the angle between the wave vectors of the gratings, and

$$\rho = k_1/k_2, \tag{13}$$

is the ratio of wave numbers which are the moduli of the corresponding wave vectors as follows, $k_1 = |\mathbf{k}_1|$, $k_2 = |\mathbf{k}_2|$. Substituting Eq. (12) into Eq. (11), we have

$$\begin{aligned} t_{123} = t_1 t_2 t_3 &= \frac{1}{16}(1 + \cos\rho k x)(1 + \cos\rho k y) \\ &\quad \times \{1 + \cos[k(x\cos\alpha + y\sin\alpha)]\} \\ &= \frac{1}{16}(1 + \cos\rho k x + \cos\rho k y + \cos\rho k x \cos\rho k y) \\ &\quad \times \{1 + \cos[k(x\cos\alpha + y\sin\alpha)]\} \\ &= \frac{1}{16}\left[1 + \cos\rho k x + \cos\rho k y + \frac{1}{2}\cos\rho(k x - k y) \right. \\ &\quad \left. + \frac{1}{2}\cos\rho(k x + k y)\right]\{1 + \cos[k(x\cos\alpha + y\sin\alpha)]\}. \end{aligned} \tag{14}$$

Similarly, applying the equation for the product of cosines several times, we have

$$\begin{aligned} t_{123} = \frac{1}{16}&[1 + \cos\rho k x + \cos\rho k y + \cos(\cos\alpha k x + \sin\alpha k y)] \\ &+ \frac{1}{32}\left\{\begin{array}{l} \cos\rho k(x - y) + \cos\rho k(x + y) \\ + \cos[(\rho + \cos\alpha)k x + \sin\alpha k y] + \cos[(\rho - \cos\alpha)k x - \sin\alpha k y] \\ + \cos[\cos\alpha k x + (\rho + \sin\alpha)k y] + \cos[-\cos\alpha k x + (\rho - \sin\alpha)k y] \end{array}\right\} \\ &+ \frac{1}{64}\left\{\begin{array}{l} \cos[(\rho + \cos\alpha)k x + (-\rho + \sin\alpha)k y] + \cos[(\rho - \cos\alpha)k x + (\rho + \sin\alpha)k y] \\ + \cos[(\rho + \cos\alpha)k x + (\rho + \sin\alpha)k y] + \cos[(\rho - \cos\alpha)k x + (\rho - \sin\alpha)k y] \end{array}\right\}. \end{aligned} \tag{15}$$

The following identity means the rotation of coordinates by the angle $\theta = \arctan b/a$

$$\cos(a x + b y) = \cos\left(\sqrt{a^2 + b^2}\, x'\right) = \cos(k x'), \tag{16}$$

where

$$k = \sqrt{a^2 + b^2}. \tag{17}$$

Applying Eq. (17) to Eq. (15), we can obtain the wave numbers of all terms of Eq. (15). These wave numbers are listed below in the same order as in Eq. (15)

$$k_i = 0, \rho, \rho, 1, \sqrt{2}\cdot\rho, \sqrt{2}\cdot\rho, \quad \sqrt{\rho^2 + 2\rho\cos\alpha + 1},$$
$$\sqrt{\rho^2 - 2\rho\cos\alpha + 1}, \quad \sqrt{\rho^2 + 2\rho\sin\alpha + 1},$$
$$\sqrt{\rho^2 - 2\rho\sin\alpha + 1}, \sqrt{2\rho^2 + 2\rho\cos\alpha - 2\rho\sin\alpha + 1},$$
$$\sqrt{2\rho^2 - 2\rho\cos\alpha + 2\rho\sin\alpha + 1},$$
$$\sqrt{2\rho^2 + 2\rho\cos\alpha + 2\rho\sin\alpha + 1},$$
$$\sqrt{2\rho^2 - 2\rho\cos\alpha - 2\rho\sin\alpha + 1}, \quad i = 1, \ldots, 14. \tag{18}$$

Equation (18) shows that there are eight different nonconstants (i.e., depending on the angle) wave numbers among 14 terms of Eq. (15).

The symmetry of the problem suggests that the angular range (domain) to be considered in the case of the square grid is [0 deg, 45 deg]. All calculations can be made within this domain only; the angles outside it can be reduced into the domain by means of finding the remainder of the division by 45.

None of eight nonconstant functions equals 0 within the domain. Only two functions fall down to 0 at the edges; the function $\sqrt{\rho^2 - 2\rho\cos\alpha + 1} = 0$ at the left edge ($\alpha = 0$) with $\rho_{01} = 0$, and the function $\sqrt{2\rho^2 - 2\rho\cos\alpha - 2\rho\sin\alpha + 1}$ at the right edge ($\alpha = 45$ deg) with $\rho_{11} = 1/\sqrt{2}$. Both cases describe infinitely long waves, which represent the strongest moiré waves because according to our visibility assumption[48] that the waves with longer periods are better visible (this assumption is confirmed later experimentally by the direct amplitude measurements[58]). The corresponding wave numbers are

$$k_{01}(\rho, \alpha) = \sqrt{\rho^2 - 2\rho\cos\alpha + 1}, \tag{19}$$

$$k_{11}(\rho, \alpha) = \sqrt{2\rho^2 - 2\rho\cos\alpha - 2\rho\sin\alpha + 1}. \tag{20}$$

The functions defined in Eqs. (19) and (20) are continuous and monotonous; one of them is rising, another falling. Therefore, they must intersect within the domain at certain α_0, and the period at that point is definitely shorter than at the edges, and the moiré patterns are less visible. Thus, the moiré patterns can be minimized.

In the left "half" of the domain ($0 < \alpha < \alpha_0$), the function defined in Eq. (19) prevails, i.e., it has lower values which correspond to the longer wavelengths. In the right "half" of the domain ($\alpha_0 < \alpha < 45$ deg), the function defined in Eq. (20) prevails. The best visible patterns at the left edge of the domain are represented by the first function. At larger angles, the visibility falls down (because the wavelength shortens) until the intersection point. After that point, the best visible patterns are represented by the second function; the visibility increases and reaches another maximum at the right edge of the domain. Therefore in general, the visibility of the moiré patterns is lowest at the intersection point α_0.

Examples of the moiré patterns are shown in Fig. 8; the corresponding gratings are shown in Fig. 7. Figure 8 shows the moiré patterns at the angles near the edges of the domain and near its middle for the size ratios of 1 and 0.707 (namely, the angles slightly deviated from 0 deg, 45 deg, and 27 deg). Note that the period of the patterns in Figs. 8(b)–8(e) is not much longer than the period of the gratings.

Let us find the intersection of the functions defined by Eqs. (19) and (20). Substitute ρ_1 mentioned above into the first function, and ρ_2 into the second one. At the intersection, the two functions are equal, i.e.,

$$\sqrt{1 - 2\cos\alpha + 1} = \sqrt{1 - \frac{2}{\sqrt{2}}\cos\alpha - \frac{2}{\sqrt{2}}\sin\alpha + 1}, \tag{21}$$

which is equivalent to the following equation:

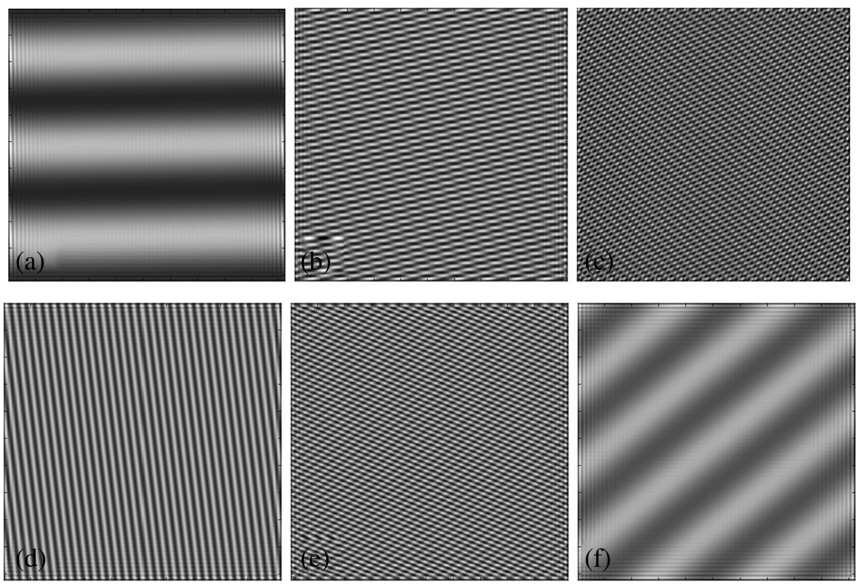

Fig. 8 Moiré patterns: size ratio 1, angles 2 deg, 27 deg, and 43 deg in (a), (b), and (c), respectively; size ratio 0.707 and the same angles in (d), (e), and (f), respectively.

$$\cos\alpha(1-\sin\alpha)=\frac{1}{2}. \tag{22}$$

For the new variable $S=\sin\alpha$, Eq. (22) can be rewritten as a quartic equation

$$S^4-2S^3+2S-\frac{3}{4}=0. \tag{23}$$

This equation has the only real root $S=0.442$ within the domain; the corresponding angle is

$$\alpha_0=26.261\ \text{deg}. \tag{24}$$

Note that this angle is very close to

$$\alpha_{1/2}=\arctan\frac{1}{2}=26.565\ \text{deg}. \tag{25}$$

(The difference between two above angles is about 1%). It means that either of two angles Eqs. (24) or (25) can be practically used in the sinusoidal approximation with the accuracy about 99%.

From a proper (long enough) distance, the short-period patterns at the angle α_0 (or $\alpha_{1/2}$) are unrecognizable and thus are effectively eliminated, see Figs. 8(b) and 8(e). For the equations in the polar coordinates refer to Ref. 59.

3.2.1 *Exercises*

1. Point out the terms of Eq. (15) responsible for the strongest functions given in Eqs. (19) and (20).
2. Write down the equation of strongest waves for the 60-deg rhomboidal grating combined with a line grating.
3. Find the period of residual moiré patterns at the optimal angle (you may use either of two branches).
4. Find the period of the moiré patterns in square grating 1 mm + line grating 1.1 mm at the angles of 0 deg, 5 deg, and 10 deg.
5. Determine the orientation of the moiré pattern in line gratings 1 mm + 1.2 mm installed at 10 deg.

4 Sinusoidal Noncoplanar Gratings

Practically, the layers may not lie in the same plane. For example, a typical structure of the autostereoscopic 3-D displays contains two parallel layers separated by an air gap. Such a nonplanar layout makes the moiré patterns alive and vivid. The visual picture may look dissimilar from different directions, and the movement of the patterns sometimes looks unexpected; moreover, their behavior may seem unpredictable. This section is based on Refs. 28 and 60. Consider two layers observed from a finite distance l as shown in Fig. 9.

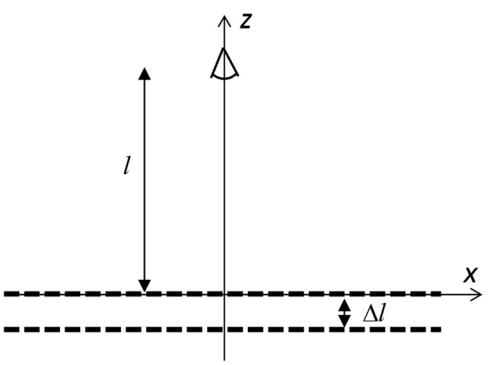

Fig. 9 Two noncoplanar layers and the observer.

According to Ref. 60, the period of the moiré patterns in this case (two line gratings) is

$$T_m=\frac{1}{\left|\frac{s}{\rho}-1\right|}T_1, \tag{26}$$

where ρ is defined in Eq. (13) and s is the geometric factor

$$s=1+\frac{\Delta l}{l}, \tag{27}$$

where l is the coordinate of the observer and Δl is the gap between the layers.

This expression for the period can be rewritten in terms of the moiré magnification factor; by its physical meaning, the moiré factor is an amplification coefficient (or a gain factor) for the period of the grating. The moiré factor corresponding to Eq. (26) is

$$\mu=\frac{1}{\left|\frac{s}{\rho}-1\right|}. \tag{28}$$

Note that when $\rho=s$, the moiré factor Eq. (28) formally reaches infinity, which means the infinitely long period. However practically, we cannot measure an infinite period. The maximum value of the period is always limited by the size of a screen, where the patterns are observed; this is because the patterns with the period longer than that screen cannot be recognized as periodic waves at all. Equation (28) is graphically shown in Fig. 10.

The particular case of Eq. (28) for the identical gratings with $\rho=1$ is as follows:

$$\mu=\frac{l}{\Delta l}. \tag{29}$$

Examples of moiré patterns are shown in Fig. 11 for the same distance, but different gaps between gratings in Figs. 11(a) and 11(b), as well as for the same gap but different distances in Figs. 11(c) and 11(d).

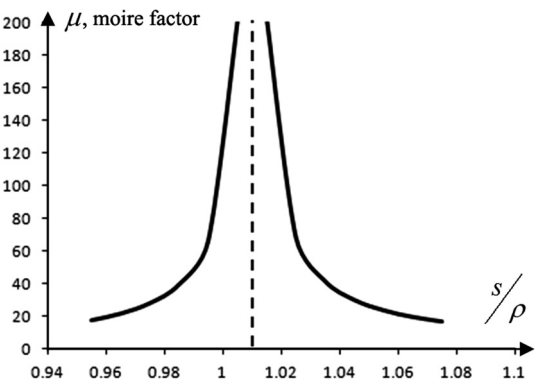

Fig. 10 Moiré factor depending on ratio s/ρ.

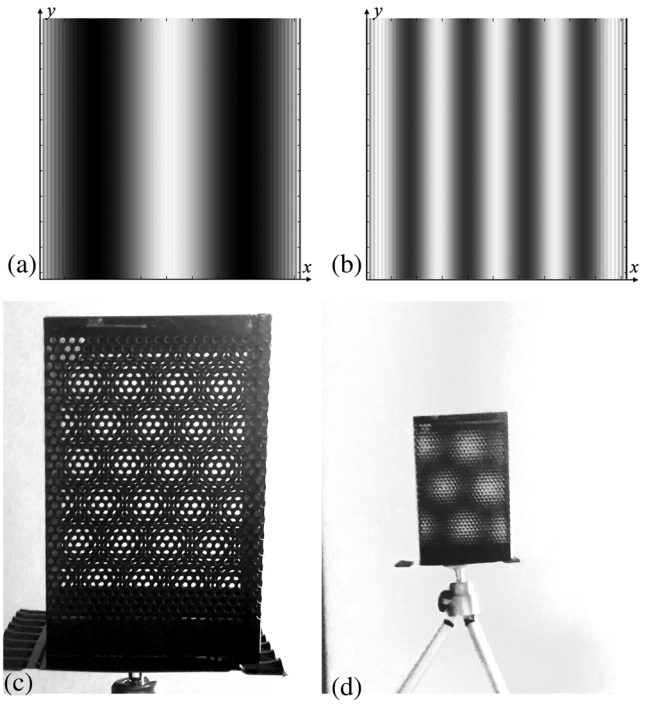

Fig. 11 Moiré patterns in identical gratings. Computer simulation of gratings with period 0.11 cm at the same distance 100 cm, but different gaps: (a) 2 cm, (b) 5 cm; one unit = 1 cm. Experimental photographs of gratings with period 0.3 cm and the same gap 7 cm, but different distances: (c) 50 cm and (d) 100 cm.

A lateral displacement of the gratings (or the camera) does not affect the period; however in this case, the patterns are displaced laterally by the following value:

$$x_m = \frac{\rho x_1 - x_2}{s - \rho}, \tag{30}$$

where x_1 and x_2 are the displacements of the gratings. The physical meaning of this equation is that the displacement of a grating by its period results in the displacement of the patterns by their period.

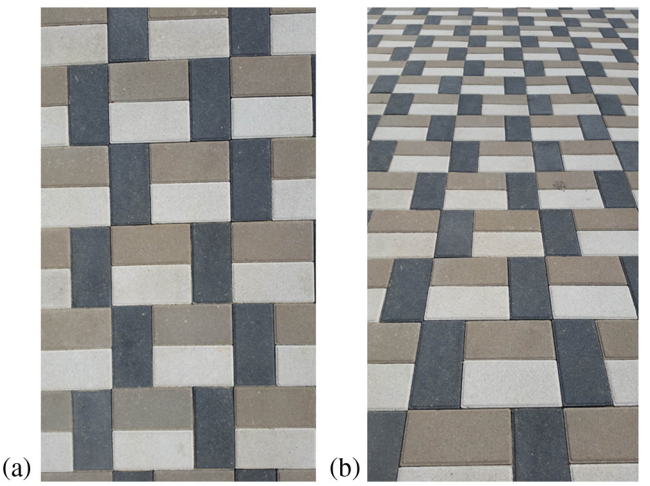

Fig. 12 Two photographs of the same pavement taken by the same camera, but from different angles.

Note that our equations were obtained for the camera axis orthogonal to the plain gratings. The picture may look completely different in an nonorthogonal case. Compare two photographs of the same plane pavement in Fig. 12 taken by the same camera, but with the different angles between the camera axis and the surface.

In the first case (the camera axis perpendicular to the surface), the shape and size of all bricks (rectangles) in the photograph are identical. In the second case (the camera with the axis deviated from the perpendicular), all quadrilaterals (projections of the rectangular bricks) are different; it means a strong dependence of their shape and size on coordinates.

4.1 *Exercises*

1. Find the period of the moiré patterns in the identical parallel gratings (period 2 mm) installed with the gap of 1, 5, and 10 mm. The observer distance is 1 m.
2. Rewrite the equation for the moiré factor using one variable only. What could be its physical meaning?
3. Determine the gap based on the moiré period for:
   a. parallel identical gratings.
   b. identical gratings in the parallel planes but installed at the angle.
4. Find the angle of the moiré image for the identical gratings in parallel planes (but not necessarily parallel orientation of gratings).
5. Obtain the homogeneous transformation matrices for the two cases shown in Fig. 12.
6. What is a condition to see the moiré patterns of the infinite period from the finite distance in the parallel players installed with a gap?
7. Is it physically possible for the moiré factor to be equal to one?

5 Cylindrical Moiré (Orthogonal Projection)

Consider a regular 3-D object: a cylinder made of a wrapped periodic mesh, see Fig. 13. This section is based on Refs. 61–63.

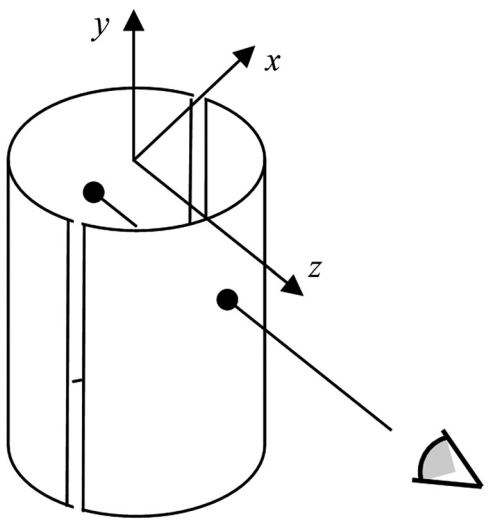

Fig. 13 Cylinder observed through both halves.

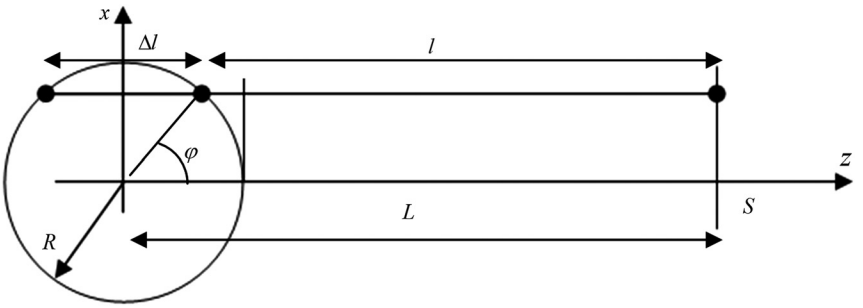

Fig. 14 Horizontal cross section of cylinder.

The cylinder can be logically split into two halves, front and rear, which are made of the same mesh. When we look through meshes with a gap between them, the moiré patterns may appear, as described in Sec. 4.

To calculate the period of the moiré patterns, we use the orthogonal projection of the points lying on the surface of the cylinder onto a screen which is parallel to the xy-plane. Correspondingly, the projection lines are always parallel to the z-axis; the coordinate x can be treated as an impact parameter. Let R be the radius of the cylinder, L the distance from the screen S to the center of the circle. An example projection line in Fig. 14 connects three circular dots, two on the circle, and one on the screen. The point, where this line crosses the x-axis, is the orthogonal projection of two points from the cylindrical surface onto the screen S.

In this section, all distances are measured along the lines parallel to the z-axis. The distance Δl between the gratings along the z-coordinate displaced by x is equal to the chord of the circle. From the equation of the cylinder, the length of the chord is

$$\Delta l = 2\sqrt{R^2 - x^2}. \tag{31}$$

Then, the distance l from the observer to the first grating is L minus one half of the chord

$$l = L - \frac{\Delta l}{2} = L - \sqrt{R^2 - x^2}. \tag{32}$$

With using the polar angle $\varphi = \arcsin(x/R)$ of polar coordinates, Eqs. (31) and (32) can be re-expressed as follows:

$$\Delta l = 2R\cos\varphi, \tag{33}$$

$$l = L - R\cos\varphi. \tag{34}$$

The variables l and Δl for Eq. (29) describing the moiré effect in the parallel noncoplanar gratings are found. However in the case of a spatial object as a cylinder, the gratings are not parallel, and therefore the orientation of the wave vector in space has to be additionally taken into account. Correspondingly, two types of gratings on the surface of the cylinder should be analyzed: the grating with the vertical wave vector orthogonal to the base of the cylinder shown in Fig. 15(a) and the grating with the horizontal wave vector parallel to the base shown in Fig. 15(b).

In the other words, the former grating consists of the identical circles uniformly displaced along the y-axis; the latter consists of the vertical lines uniformly distributed along the circle, the base of the cylinder. These two cases are well separated (this fact is confirmed experimentally in Ref. 61) and therefore can be considered in isolation from one another.

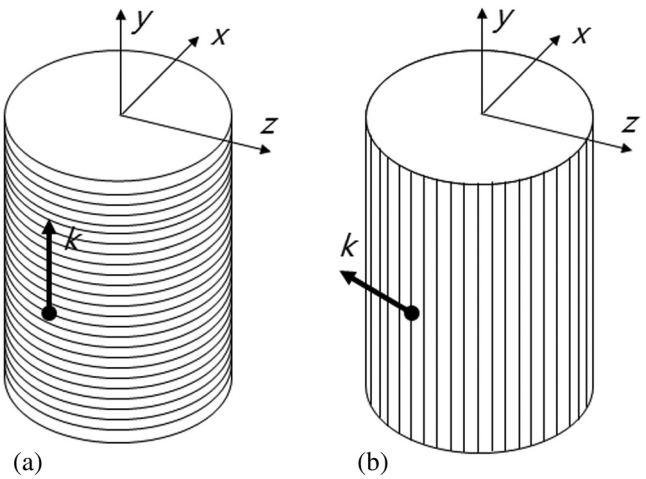

Fig. 15 Wave vectors of two types of gratings on the cylinder (a) vertical wave vector and (b) horizontal wave vector.

In the orthogonal projection of the first grating onto the yz-plane, the projected period is equal to the period of the grating, see Fig. 16(a). However, the projected period of the second grating is not constant along the x-axis, as shown in Fig. 16(b), and depends on the local inclination of the cylindrical surface, which is proportional to the cosine of the polar angle. Therefore in this case, the projected period should be multiplied by $\cos\varphi$.

Based on Eqs. (33) and (34), the moiré periods of these cases are calculated as follows:

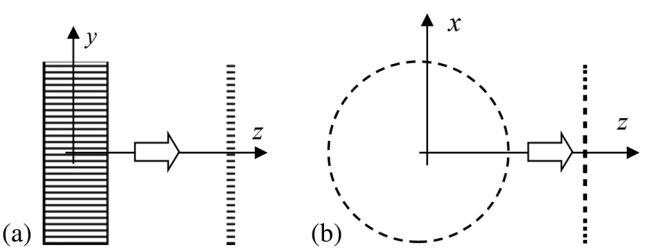

Fig. 16 Orthogonal projections of two types of gratings onto the screen parallel to xy-plane: (a) vertical wave vector and (b) horizontal wave vector.

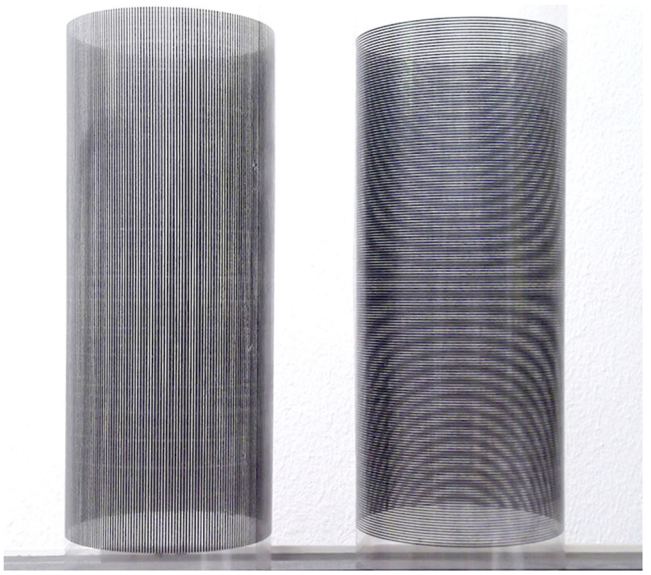

Fig. 17 Experimental photographs of the moiré patterns in two types of gratings.

$$T_v = \frac{l}{\Delta l} = \frac{T}{2}\left(\frac{L}{R\cos\varphi} - 1\right), \tag{35}$$

$$T_h = \frac{l}{\Delta l}\cos\varphi = \frac{T}{2}\left(\frac{L}{R} - \cos\varphi\right). \tag{36}$$

The photographs of the moiré patterns in cylinders with the horizontal and vertical wave vectors are shown in Fig. 17.

The corresponding moiré magnification factors are given by the following equations:

$$\mu_v = \frac{1}{2}\left(\frac{L}{R\cos\varphi} - 1\right), \tag{37}$$

$$\mu_h = \frac{1}{2}\left(\frac{L}{R} - \cos\varphi\right). \tag{38}$$

A graphical illustration of the theoretical dependences Eqs. (37) and (38) is shown in Fig. 18. Note that $\cos\varphi = x/R$. Across the radius, the horizontal moiré factor deviates <1%, whereas the vertical one raises more than twice.

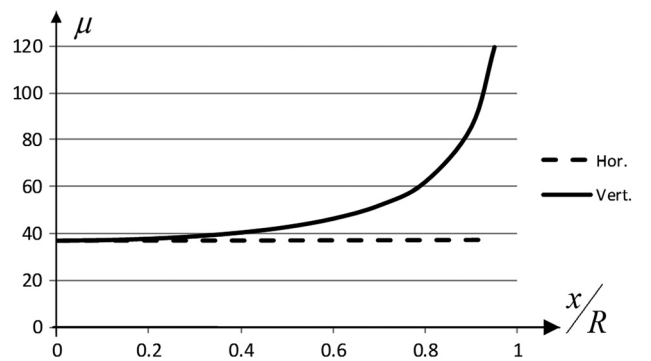

Fig. 18 Theoretical moiré factors in cylindrical objects for two orthogonal wave vectors ($L/R = 75$).

5.1 *Exercises*

1. The period of the moiré patterns for the grating period 1 mm and the diameter 10 and 20 mm; the observer distance is 0.5 m.
2. Draw a sketch of the patterns in wrapped skew gratings (neither vertical nor horizontal layout, but an intermediate inclination angle between 0 deg and 90 deg) based on Eqs. (35) and (36).
3. Compare the periods of the moiré patterns on the axis of the cylinder for the grating with the lines parallel to the axis of the cylinder and for the inclined grating with the correspondingly inclined parallel gratings (their gap = diameter of the cylinder).

6 Moiré Wave Vector as a Vector Sum

Now, consider the moiré effect in the spectral domain, where we deal with the reciprocal distances or, equivalently, with the wave vectors.

Generally speaking, the wave vector of the moiré patterns is that linear combination of the wave vectors of gratings (with coefficients +1 and −1), which is closest to the origin. It means either the sum or the difference; whichever is shorter, see Fig. 19. Typically (but not always), it is the difference between the wave vectors of two gratings.

Let $\mathbf{k}_1$ and $\mathbf{k}_2$ be the wave vectors of the gratings and α the angle between them. Based on these vectors, we will find the moiré wave vector $\mathbf{k}_m$ and the moiré orientation angle θ. Figure 19 is an illustration for the wave vectors with close wave numbers but different orientations.

It can be seen that for close wave numbers and $\alpha > 90$ deg, it is the summation; otherwise (i.e., when $\alpha < 90$ deg), it is the subtraction. Figure 19(b) actually shows the layout of the wave vectors for Eq. (10) in Sec. 3.

Figure 20 shows the map of the spectrum of two overlapped sinusoidal gratings [Fig. 19(b)]. Among all combinational components, the linear combination with the smallest wave number is the moiré wave vector.

The extremely important concept of the visibility circle[1] models the human visual system in the spectral domain. The visible vectors lie within the visibility circle, the vectors outside the visibility circle are invisible, see Fig. 21.

Consider the triangle with the sides $\mathbf{k}_1$ and $\mathbf{k}_m$ and the angle $2\pi - \theta$ between them in the case of the subtraction shown in Fig. 19(b). From the law of cosines for the side $\mathbf{k}_2$

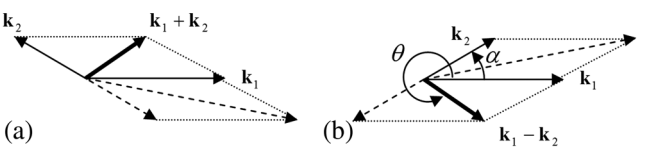

Fig. 19 The moiré wave vector in two layouts of the wave vectors of gratings: (a) sum and (b) difference.

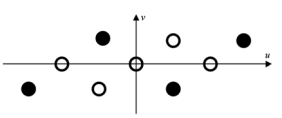

Fig. 20 Map of spectrum (all linear combinations of wave vectors) of two overlapped sinusoidal gratings.

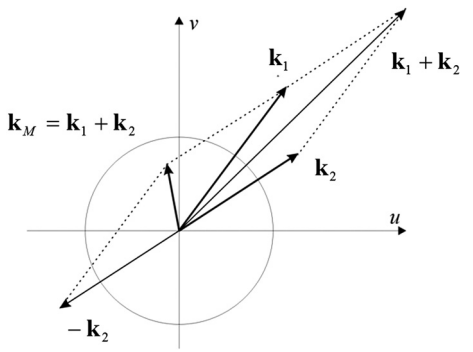

Fig. 21 Moiré wave vector and visibility circle.

$$k_2^2 = k_1^2 + k_m^2 - 2k_1 k_m \cos(2\pi - \theta) \tag{39}$$

and

$$\cos(2\pi - \theta) = \frac{k_1^2 + k_m^2 - k_2^2}{2k_1 k_m}. \tag{40}$$

Similarly to the wave numbers k_1 and k_2 in Eq. (13), $k_m = |\mathbf{k}_m|$.

From the law of cosines for the side $\mathbf{k}_m$, we have the modulus of the moiré wave vector

$$k_m^2 = k_1^2 + k_2^2 - 2k_1 k_2 \cos\alpha \tag{41}$$

and accordingly

$$\cos(2\pi - \theta) = \frac{k_1 - k_2 \cos\alpha}{\sqrt{k_1^2 + k_2^2 - 2k_1 k_2 \cos\alpha}}. \tag{42}$$

Therefore,

$$\sin(2\pi - \theta) = \sqrt{1 - \cos^2(2\pi - \theta)} = \frac{k_2 \sin\alpha}{\sqrt{k_1^2 + k_2^2 - 2k_1 k_2 \cos\alpha}}. \tag{43}$$

Recall that

$$\sin\theta = -\sin(2\pi - \theta), \tag{44}$$

$$\cos\theta = \cos(2\pi - \theta). \tag{45}$$

Thus, the orientation of the wave vector of the moiré patterns is

$$\tan\theta = \frac{\sin\theta}{\cos\theta} = \frac{-\sin(2\pi - \theta)}{\cos(2\pi - \theta)} = -\frac{k_2 \sin\alpha}{k_1 - k_2 \cos\alpha}. \tag{46}$$

The two Eqs. (41) and (46) comprise the full solution (the wave number and the orientation).

The relation for the periods is an inverse wave vector Eq. (41)

$$T_m = \frac{T_1 T_2}{\sqrt{T_1^2 + T_2^2 - 2T_1 T_2 \cos\alpha}}. \tag{47}$$

The orientation Eq. (46) can be also rewritten in terms of the periods

$$\tan\theta = -\frac{\frac{1}{T_2}\sin\alpha}{\frac{1}{T_1} - \frac{1}{T_2}\cos\alpha} = -\frac{T_1 \sin\alpha}{T_2 - T_1 \cos\alpha}. \tag{48}$$

This is actually the same expression as Eq. (6) in Sec. 2. Moreover, Eqs. (47) and (48) can be re-expressed in terms of the ratio of periods $\rho = T_2/T_1$ [compare with the definition Eq. (13) in Sec. 3.2] as follows:

$$T_m = T_2 \frac{1}{\sqrt{1 + \rho^2 - 2\rho\cos\alpha}}, \tag{49}$$

$$\tan\theta = \frac{\sin\alpha}{\rho - \cos\alpha}. \tag{50}$$

Furthermore, Eq. (49) can be expressed in terms of the moiré factor

$$\mu = \frac{1}{\sqrt{1 + \rho^2 - 2\rho\cos\alpha}}. \tag{51}$$

6.1 *Exercises*

1. Rewrite the expression for the wave vector using the ratio of wave numbers.
2. Determine the minimum/maximum period from Eq. (49) depending on the angle.
3. Draw the moiré wave vector for three line gratings of arbitrary periods and angles.
4. Find the orientation of the moiré patterns at min/max period from exercise 2.

7 Basics of Two-Dimensional Fourier Transform

7.1 *Spectra*

A relation between variables can be described mathematically in two ways: either by the functional dependence or by the spectrum; corresponding examples are given in Fig. 22. Both ways characterize the same relation from different perspectives. For example, Figs. 22(a) and 22(b) describe the sinusoidal wave, whereas Figs. 22(c) and 22(d) the square wave.

The Fourier spectra of real symmetric functions are real and symmetric, although in general, the spectra of arbitrary functions (including the real but nonsymmetric functions) are complex. In the tutorial we consider the power spectra,

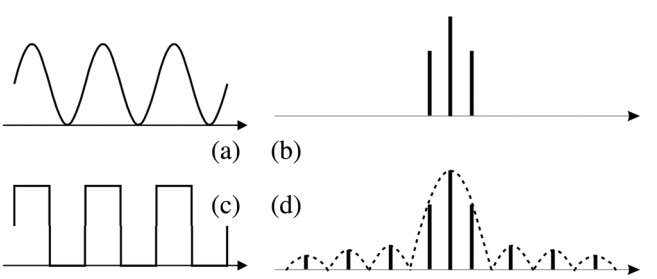

Fig. 22 1-D functions (sinusoidal and square waves) and their power spectra: (a) sinusoidal function and (b) its spectrum of the right column, (c) square function, and (d) its spectrum of the right column.

i.e., the modules of the Fourier coefficients, which are always real. For the periodic sinusoidal f_1 and rectangular f_2 functions shown in Fig. 22, we have

$$f_1(x) = \frac{1}{2} + \sin\, kx, \tag{52}$$

$$\begin{cases} f_2(x) = \begin{cases} 1, & |x| < 1/2 \\ 0, & 1/2 < |x| < 1 \end{cases}, \\ f_2(x+T) = f_2(x) \end{cases} \tag{53}$$

and the corresponding spectra are

$$F_1(k) = \frac{1}{2} + \frac{\delta(k) + \delta(-k)}{4}, \tag{54}$$

$$F_2(k) = \frac{1}{2} + \frac{2}{\pi} \sum_{n=1,3,5,\ldots}^{\infty} \frac{1}{n} \sin(2\pi n k). \tag{55}$$

The previous expression can be rewritten in terms of sinc function defined as follows:

$$\mathrm{sinc}(x) = \frac{\sin(x)}{x}. \tag{56}$$

(Sometimes you can meet an alternative definition $\mathrm{sinc}(x) = \sin(\pi x)/\pi x$ which differs in the normalization of the coordinate.) The rewritten Eq. (55) is as follows:

$$F_2(k) = \frac{1}{2} + 4k \sum_{n=1,3,5,\ldots}^{\infty} \mathrm{sinc}(2\pi n k). \tag{57}$$

The sinusoidal grating has three spectral components (one of them is a constant term, while two others represent a sinusoidal wave itself). The rectangular grating has many spectral components; theoretically, an infinite number of the decayed components. The decay rate of the Fourier coefficients depends on the smoothness of the function[64] and particularly, for a piecewise continuous function is $1/n$. The spectrum of a symmetric square wave contains only odd harmonic frequencies, see Fig. 22(d), where all even harmonics are equal to zero. Figure 22(b) shows that the power spectrum of a sinusoidal grating can be thought as a limited (central) part of the spectrum of a rectangular grating.

7.2 *Two-Dimensional Spectra*

Figure 22 of the previous section shows the 1-D functions. A 1-D function of one variable (graphically, the "height" y as a function of the abscissa x) can be generalized to a 2-D function of two variables (the "height" z as a function of two independent coordinates x and y).

The 2-D case looks somewhat complicated, but not very sophisticated and still understandable. In two dimensions, the spectrum of a line grating is spread along a slant straight line (an abscissa of a 1-D spectrum) and repeated (copied) in the orthogonal direction. A 2-D function represents a surface and can be displayed, for instance, as a "map" with colors for the height; the white color may mean the lowest value (say, zero), while the black color means the highest value (say, one). Such maps of the plane waves (sinusoidal and square profile) are drawn in Figs. 23(a) and 23(c) together with their profiles; the spectra are shown in Figs. 23(b) and 23(d), respectively.

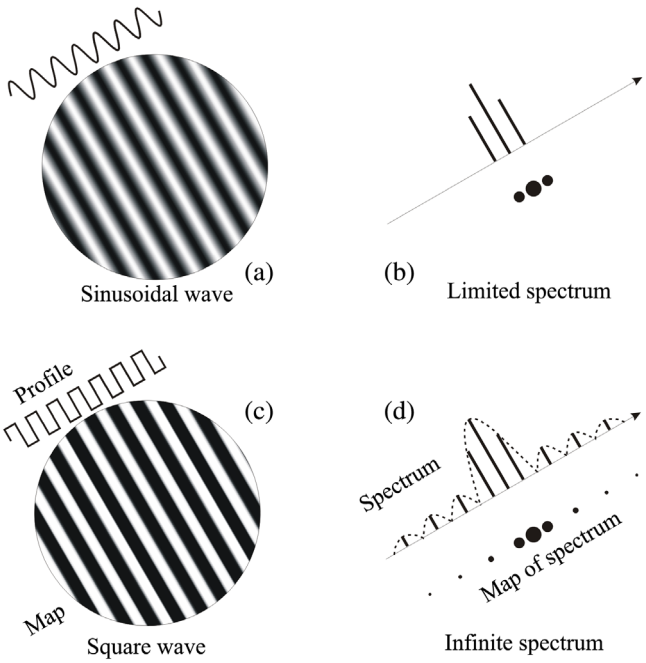

Fig. 23 2-D functions (sinusoidal and square waves) and their power spectra.

In many cases, a 2-D grid can be represented as a product of two 1-D gratings. For illustration, refer to Fig. 7 and to Eqs. (10) and (11). Many useful details about discrete transforms can be found in Ref. 56.

7.2.1 *Exercises*

1. Describe the spectrum of the sinusoidal square grid (which is a superposition of two line gratings).
2. Describe the spectrum of the nonsinusoidal square grid.
3. Draw the map of peaks for three superposed sinusoidal gratings at the angle near 60 deg.
4. What is the 2-D Fourier transform of two orthogonal gratings with the periodic triangular transparency function?
5. How to find the phase of the wave from the Fourier coefficients?
6. Distance between the spectral peaks of the function $\sin(3x + 4y)$.

8 Spectral Trajectories

Generally speaking, parameters of the gratings do not always remain constant and may change. This change causes the change of the spectrum. In the case of an incremental change of a parameter, a set of several spectra represents a richer picture of the behavior of the patterns. For example, when a sinusoidal line grating whose initial spectrum is shown in Fig. 24(a) turned around, its spectrum is also rotated, see Fig. 24(b). Several overlapped spectra of an incrementally rotated grating are shown in Fig. 24(c) for the angles 0 deg to 40 deg with increment 5 deg; these look like

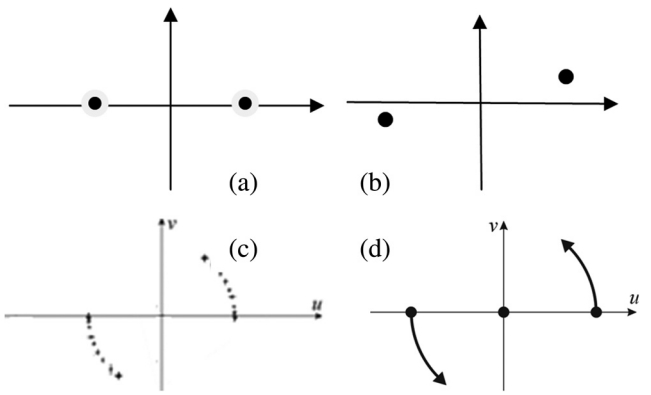

Fig. 24 Spectra of one rotated grating (a) initial grating, (b) rotated grating, (c) overlapped spectra of grating rotated by several angles, and (d) scheme of spectra (spectral trajectory).

a set of discrete points. Schematically, such sets of spectra can be drawn by continuous trajectories in the spectral domain, see Fig. 24(d).

Furthermore, one may consider the spectral domain with the axes u, v as the complex plane with u and v as the real and the imaginary parts of a complex number z. Then, all locations and shapes in the complex plane and spectral domain are identical, but the calculations become convenient and simple because the complex numbers allow applying many powerful mathematical theorems.

This section is based on Ref. 57. Consider a superposition of two rectangular grids, which can be often met in practice. The equation of the spectral peaks of four gratings arranged in two layers (each layer consists of two orthogonal gratings) is

$$T_{2\times 2} = k(p_1\sigma_1 + ip_2) + k\rho(p_3\sigma_3 + ip_4)e^{i\alpha}, \tag{58}$$

where $p_1, \ldots, p_4$ are integer numbers numbering the harmonics of each of four gratings, σ_1 and σ_3 are aspect ratios of the rectangular gratings in two layers (for the square gratings, $\sigma_1 = \sigma_3 = 1$), and ρ is the size ratio as that in Eq. (13) in Sec. 3. The general equation of the spectral peaks and the equations for other superpositions can be found in Ref. 57.

A picture of trajectories Fig. 24(d) shows where the spectral peaks can be located when the angle varies. The spectral trajectories are known in many areas, refer, for instance, to Refs. 65 and 66. For the moiré effect, the spectral trajectories were first time proposed in Ref. 57.

In the case of two square gratings and the running angle, the trajectory derived from Eq. (58) is as follows:

$$T_{2\times 2\alpha}(t) = (p_1 + ip_2)k + (p_3 + ip_4)k\rho e^{i\alpha(t)}. \tag{59}$$

It can be proven that the trajectories [Eq. (59)] are either circular arcs or segments of straight lines. Different dimensions of gratings (implying that a line grating is a 1-D structure, the square grid is a 2-D structure) yield two particular cases

$$T_{2\times 2\alpha 11}(t) = p_1 k + p_3 k\rho e^{i\alpha(t)}, \tag{60}$$

$$T_{2\times 2\alpha 21}(t) = (p_1 + ip_2)k + p_3 k\rho e^{i\alpha(t)}. \tag{61}$$

The trajectories for two line gratings and two square grids [Eqs. (60) and (59)] are shown in Fig. 25. These trajectories were observed in experiments.[57] Many examples of trajectories of the sinusoidal gratings for other running parameters can be found in Ref. 67.

For the moiré effect, it is important that there can be trajectories leaving the visibility circle, approaching, entering, or crossing it, as well as the trajectories always outside or always inside the visibility circle. The visibility circle is shown in Fig. 25 by thin dashed line.

8.1 *Exercises*

1. Draw a map of peaks in the case of three overlapped sinusoidal gratings installed at the angle near 60 deg.
2. The same for 30 deg.
3. Draw a sketch of the spectral trajectories of two line gratings for the running parameter ρ and the angles $\alpha = 15$ deg, and $\alpha = 20$ deg.
4. Write equations of trajectories leaving the origin in Fig. 25(a).
5. Find the distance to the origin for the trajectories approaching the origin in Fig. 25(b).

9 Visual Effects on the Move and on the Rotation

In the case of a laterally moved 1-D grating, the corresponding displacement of the visible moiré patterns is also lateral

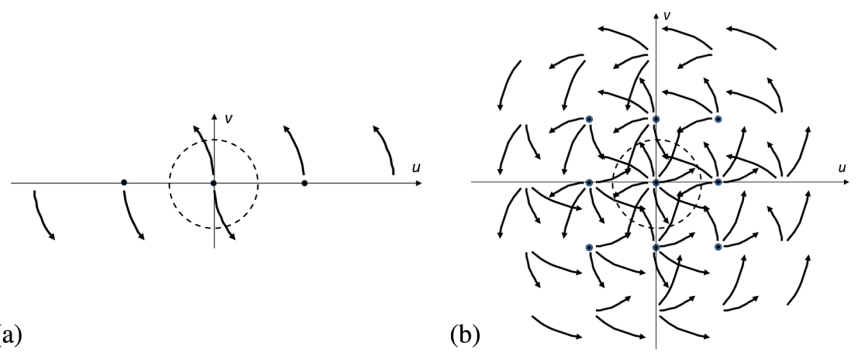

Fig. 25 Trajectories [Eqs. (59) and (60)] for sinusoidal gratings (a) two line gratings and (b) two square grids. (Running angle α between 5 deg and 40 deg, $\rho = \sigma_1 = \sigma_2 = 1$).

and given by Eq. (30) in Sec. 4. Similarly, the equation for displacement of the visible moiré patterns in the case of the moved observer can be derived from Ref. 60 as follows:

$$x_m^0 = \frac{s-1}{s-\rho} x_c. \tag{62}$$

In both cases (the moved grating or the moved observer), the displacement of the moved object by one of its periods causes the displacement of the visual picture by one period of the moiré patterns. This visual picture repeats periodically. Correspondingly, the laterally moved observer will repeatedly see the same visual picture at each period of the patterns.

In the case of identical gratings ($\rho = 1$), we have from Eq. (62)

$$x_m^0 = x_c. \tag{63}$$

Equation (63) represents so-called moiré mirror effect in the identical gratings, which results in the displacement of the moiré patterns equal to the displacement of an observer; i.e., the patterns literally follow the observer's movement, as his/her reflection in a plain mirror, see Fig. 26.

When the gratings are turned around, i.e., the angle between the gratings changes, the period of the moiré patterns also changes. In the case of the sinusoidal square gratings, almost certainly there could be two maxima at 0 and at 45 deg. For nonsinusoidal gratings, there could be several maxima at the intermediate rational angles (whose tangents are rational numbers).

At the maxima, the axis of the moiré patterns is parallel to the axis of the rotated grating and their period is maximal.[68] This can be explained in the following way. Although the spectral trajectory passes the neighborhood of the origin, the wave number reaches a minimum at that point, where the trajectory crosses the line connecting the origin and the center of the trajectory.

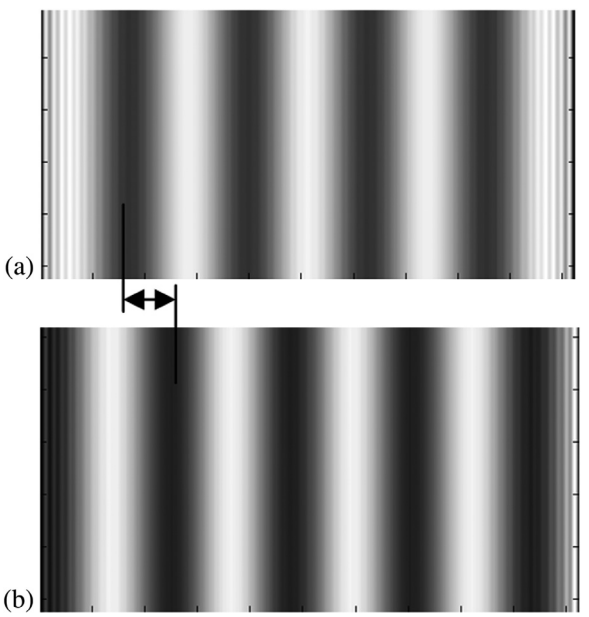

Fig. 26 Lateral displacement of the moiré patterns due to displacement of camera (a) on-axis camera, (b) off-axis (displaced) camera at the same distance. The patterns are shifted according to Eq. (63); the shift = lateral displacement of the observer.

According to Eq. (26), the period remains finite for any relation between the parameters ρ and s, except for the case of $\rho = s$. In other words, the maximum period characterizes the relation between ρ and s. From this perspective, the value of the maximum magnification factor gives an estimate of this relation. Theoretically, the maximum period depends on the particular ratio of periods of the gratings, and for the coplanar gratings with the integer ratios, the period of the moiré patterns is infinite. There can exist several local maxima. For illustration, refer to the computer simulation.[69]

The moiré factor can only be infinite in the gratings with parallel wave vectors, when $\rho = s$, i.e.,

$$\rho = 1 + \frac{d}{z} \tag{64}$$

or

$$z = \frac{d}{\rho - 1}. \tag{65}$$

This means that to obtain the infinite moiré factor, the size should correspond to the distance and gap. Before and after the "critical" distance, the moiré factor is finite. When a long-distance observer approaches to the gratings, the moiré factor increases, then reaches infinity at the critical distance, and finally decreases.

In the identical gratings at zero angle ($\alpha = 0$), the patterns are parallel to the gratings and the moiré factor is equal to z/d.

In identical gratings ($\rho = 1$) with an arbitrary angle, both moiré factor and orientation vary as follows:

$$\mu = \frac{1}{\sqrt{1 + s^2 - 2s\cos\alpha}}, \tag{66}$$

$$\tan\varphi = \frac{s\sin\alpha}{s\cos\alpha - 1}. \tag{67}$$

These equations mean that at a long distance, the moiré factor can be large, depending on the angle. When the observer approaches, the moiré factor drops down practically to zero, always remaining finite. On that move (approach), the moiré patterns rotate by ~90 deg from almost orthogonal orientation to the parallel one.

These situations can be graphically illustrated as follows. The moiré factor in the identical gratings as a function of the distance under two conditions: $d = \text{const}$ with α parameter is shown in Fig. 27; the graphs for $\alpha = \text{const}$ with d parameter look similar.

In nonidentical gratings, the moiré factor theoretically can reach the infinity. The cases of nonidentical gratings (with α as parameter) and the parallel gratings (with ρ as parameter) installed at the gap $d = 1$ are shown in Fig. 28. In the latter case, the moiré orientation is unchanged because practically we cannot distinguish between the directions 0 deg and 180 deg.

The moiré factor and the orientation of the moiré patterns in the nonidentical gratings installed at a small angle are shown in Fig. 29.

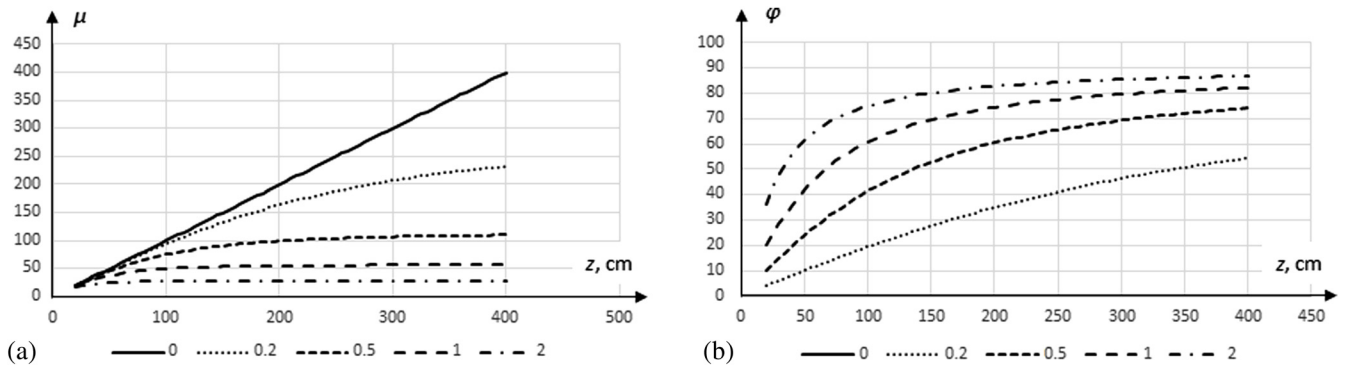

Fig. 27 (a) Moiré factor and (b) orientation in identical gratings. (The angle φ in degrees.)

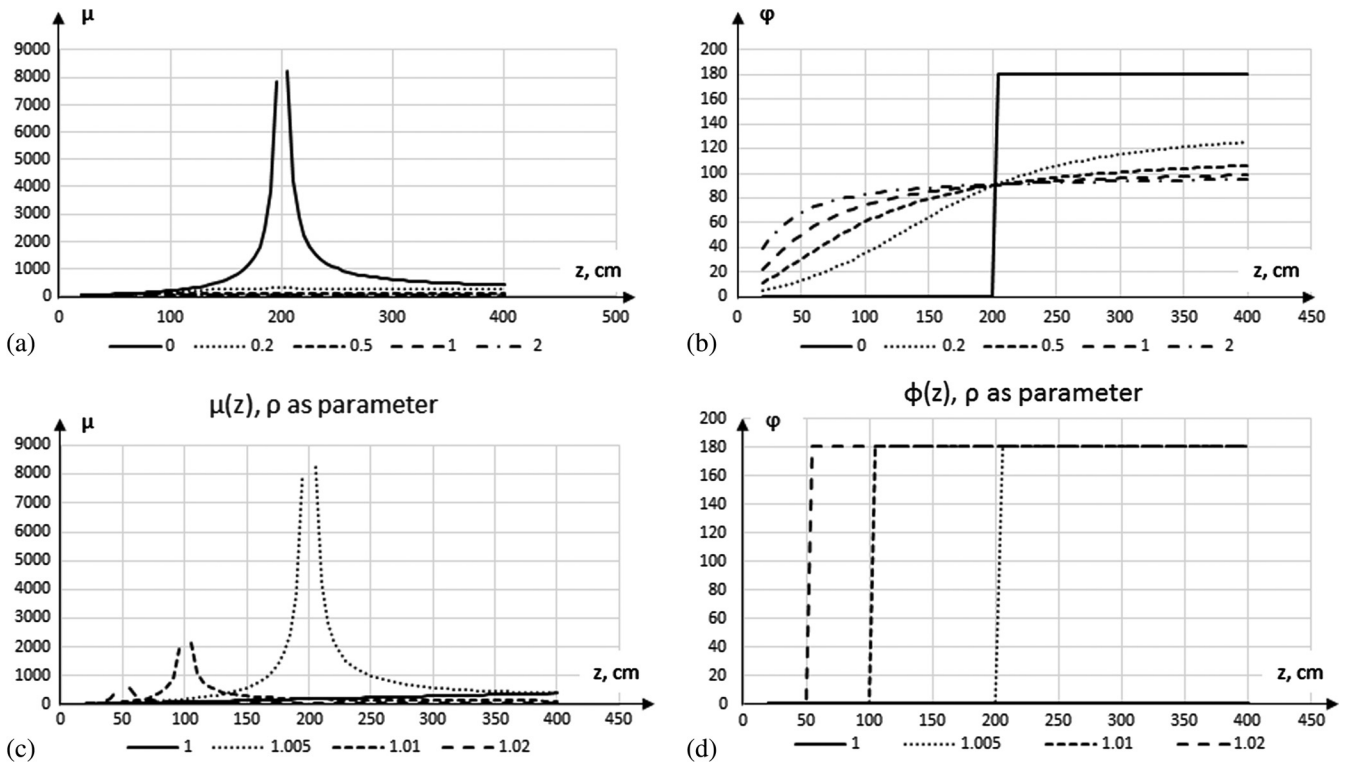

Fig. 28 (a) Moiré factor and (b) orientation in nonidentical gratings. Moiré factor (c) and orientation (d) in parallel gratings. (The angle φ in degrees.)

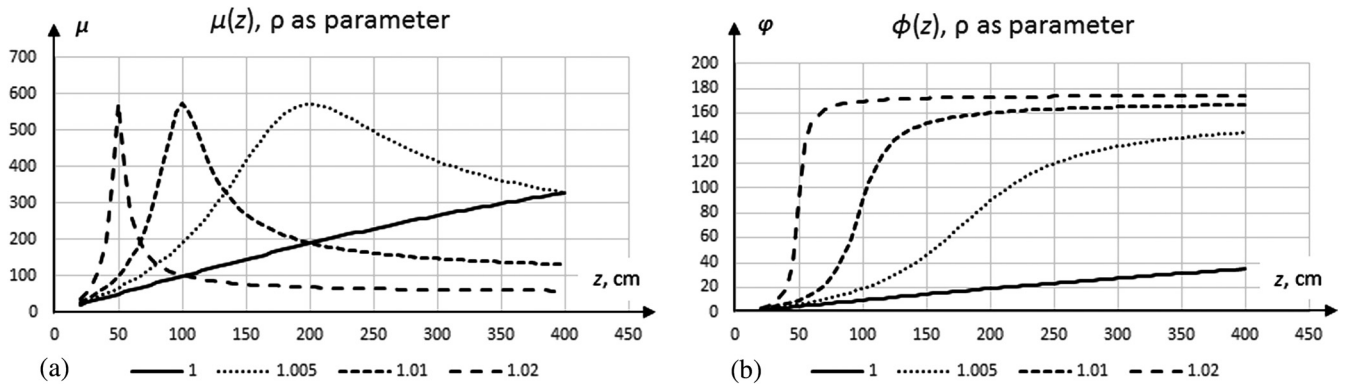

Fig. 29 Moiré factor and orientation in nonidentical skew gratings in (a) and (b), respectively. (The angle φ in degrees.)

9.1 *Exercises*

1. Make a drawing of the square grid combined with the line grating near the angle of 45 deg. Describe the visual picture of the moiré patterns for a specific ratio of periods.
2. Describe the period of the moiré patterns in the gratings when the observer approaches the screen; consider the coplanar and noncoplanar gratings.
3. Describe the moiré picture for noncoplanar square grids.
4. Can two observers see identical moiré images, if they stand shoulder to shoulder? Behind each other?

10 Discussion and Conclusion

The tutorial covers several approaches to understand the moiré effect, to study it, and, particularly, to obtain the characteristics of the visible moiré patterns in the spatial and spectral domains. The physical meaning of equations is explained. The cross references between sections are made. The experimental evidences are provided in figures.

The following topics are covered: the indicial equation, the moiré wave vector, the sinusoidal coplanar and noncoplanar gratings, the moiré effect in the cylinder, as well as the 2-D Fourier transform, the moiré spectra, and the spectral trajectories. The visual effects in the displaced or rotated gratings are discussed. These topics collected in one article describe the moiré effect from various perspectives in a variety of scenarios. This gives readers a flexible opportunity to find solutions of practical problems using this or that approach.

For further reading, we would like to provide some additional references to the moiré effect in displays.[70–72] Amazing, but the moiré effect, traditionally considered as a negative visual effect in displays, can be used to generate images including 3-D, refer to Refs. 38, 39, and 73. The color moiré effect is not considered in the tutorial. However, somebody interested can continue reading (Refs. 74–78).

As far as the gap effect is concerned, the paper[28] is already mentioned. Some more papers on the gap effect must be mentioned, too, Refs. 79–81. The related moiré rotation effect is considered in Ref. 82.

Many sources on the moiré art are available.[83–85] Among the books related to the moiré art, we would highly recommend the book,[4] as well as a good interactive illustration.[86] There are several modern painters and artists such as A. Minini, P. Dickens, P. Decrauzat, and C. Cruz-Diez, who use the moiré effect in their works; many of them are presented on the websites.[87–90]

The tutorial is intended for a wide audience, from beginners to specialists. Someone discovers the beauty of the moiré effect; someone finds details of the patterns, somebody else reveals a new approach. The authors believe that the tutorial can be useful for everybody who would read it.

Acknowledgments

This work was partially supported by the Cross-Ministry Giga KOREA Project through the Korean Government, Ministry of Science and ICT (MSIT); Grant No. GK17D0200, Development of Super Multi-View Display Providing Real-Time Interaction.

References

1. I. Amidror, *The Theory of the Moiré Phenomenon, Volume I: Periodic Layers*, 2nd ed., Springer-Verlag, London, United Kingdom (2009).
2. K. Patorsky and M. Kujawinska, *Handbook of the Moiré Fringe Technique*, Elsevier, Amsterdam, The Netherland (1993).
3. C. A. Walker, *Handbook of Moiré Measurement*, IOP Publishing, Bristol, Pennsylvania (2004).
4. N. Carsten, *Moiré Index*, Gestalten Verlag, Berlin (2010).
5. O. Bryngdahl, "Moiré: formation and interpretation," *J. Opt. Soc. Am.* **64**(10), 1287–1294 (1974).
6. S. Yokozeki, "Theoretical interpretation of the moiré pattern," *Opt. Commun.* **11**(4), 378–381 (1974).
7. S. Yokozeki, Y. Kusaka, and K. Patorski, "Geometric parameters of moiré fringes," *Appl. Opt.* **15**(9), 2223–2227 (1976).
8. C. A. Sciammarella, "The moiré method—a review," *Exp. Mech.* **22**(11), 418–433 (1982).
9. P. A. M. dos Santos, "Moiré-like patterns as a spatial beat frequency in photorefractive sinusoidal phase gratings superposition," *Opt. Commun.* **212**(4–6), 211–216 (2002).
10. O. Kafri and I. Glatt, *The Physics of Moiré Metrology*, Wiley, New York (1990).
11. M. C. Hutley et al., "Moiré magnifier," *Pure Appl. Opt.* **3**, 133–142 (1994).
12. M. Dohnal, "Moiré in a scanned image," *Proc. SPIE* **4016**, 166–170 (1999).
13. Y. Kim et al., "Color moiré pattern simulation and analysis in three-dimensional integral imaging for finding the moiré-reduced tilted angle of a lens array," *Appl. Opt.* **48**(11), 2178–2187 (2009).
14. J.-Y. Son et al., "Moiré pattern reduction in full-parallax autostereoscopic imaging systems using two crossed lenticular plates as a viewing zone forming optics," in *Proc. 10th Int. Display Research Workshops (IDW)*, pp. 1401–1404 (2003).
15. J.-Y. Son and B. Javidi, "Three-dimensional imaging systems based on multiview images," *J. Disp. Technol.* **1**(1), 125–140 (2005).
16. A. Stern and B. Javidi, "Three-dimensional image sensing, visualization, and processing using integral imaging," *Proc. IEEE* **94**(3), 591–607 (2006).
17. N. S. Holliman, "Three-dimensional display systems," Chapter C2.6 in *Handbook of Optoelectronics*, J. P. Dakin and R. G. W. Brown, Eds., pp. 1067–1100, Taylor & Francis, London, United Kingdom (2006).
18. G. Bell, R. Craig, and T. Simmiss, "Moiré interference in multilayered displays," *J. Soc. Inf. Disp.* **15**(11), 883–888 (2007).
19. R. Martinez-Cuenca et al., "Progress in 3-D multiperspective display by integral imaging," *Proc. IEEE* **97**(6), 1067–1077 (2009).
20. J.-Y. Son et al., "Recent developments in 3-D imaging technologies," *J. Disp. Technol.* **6**(10), 394–403 (2010).
21. J. Hong et al., "Three-dimensional display technologies of recent interest: principles, status, and issues," *Appl. Opt.* **50**(34), H87–H115 (2011).
22. L. Kong, G. Jin, and T. Wang, "Analysis of moiré minimization in autostereoscopic parallax displays," *Opt. Express* **21**(22), 26068–26079 (2013).
23. G. A. Bassett, J. W. Menter, and D. W. Pashley, "Moiré patterns on electron micrographs, and their application to the study of dislocations in metals," *Proc. R. Soc. London Ser. A* **246**(1246), 345–368 (1958).
24. Y. Hongbing et al., "Measurement on infrared radiation burning temperature field with moiré deviation tomography," *Microwave Opt. Technol. Lett.* **49**(11), 2761–2763 (2007).
25. U. Bonse, W. Grae, and G. Materlik, "X-ray interferometry and lattice parameter investigation," *Rev. Phys. Appl.* **11**(1), 83–87 (1976).
26. D. L. Miller et al., "Structural analysis of multilayer graphene via atomic moiré interferometry," *Phys. Rev. B* **81**, 125427 (2010).
27. G. L. Rogers, "A simple method of calculating moiré patterns," *Proc. Phys. Soc.* **73**(1), 142–144 (1959).
28. C. A. Sciammarella and F.-P. Chiang, "Gap effect on moiré patterns," *Z. Angew. Math. Phys.* **19**(2), 326–333 (1968).
29. O. Bryngdahl, "Characteristics of superposed patterns in optics," *J. Opt. Soc. Am.* **66**(2), 87–94 (1976).
30. K. Patorski, S. Yokozeki, and T. Suzuki, "Moiré profile prediction by using Fourier series formalism," *Jpn. J. Appl. Phys.* **15**(3), 443–456 (1976).
31. S. Yokozeki, "Moiré fringes," *Opt. Laser Eng.* **3**(1), 15–27 (1982).
32. C. A. Sciammarella, "Basic optical law in the interpretation of moiré patterns applied to the analysis of strains—Part 1," *Exp. Mech.* **5**(5), 154–160 (1965).
33. P. S. Theocaris, "Moiré topography of curved surfaces," *Exp. Mech.* **7**(7), 289–296 (1967).
34. P. S. Theocaris and S. A. Paipetis, "Vibration measurements by the moiré method," *J. Phys. E Sci. Instrum.* **5**(3), 217–219 (1972).
35. K. Creath and J. C. Wyant, "Moiré and fringe projection techniques," Chapter 16 in *Optical Shop Testing*, D. Malakara, Ed., pp. 653–685, John Wiley & Sons, New York (1992).

36. J. Bartl, R. Fira, and M. Hain, "Inspection of surface by the moiré method," *Meas. Sci. Rev.* **1**(3), 29–32 (2001).
37. G. N. de Oliveira, M. E. de Oliveira, and P. A. M. dos Santos, "Dynamic moiré patterns for profilometry applications," *J. Phys. Conf. Ser.* **274**(1), 012036 (2011).
38. V. Saveljev and S.-K. Kim, "A 3D moiré display," in *Proc. 33rd Int. Display Research Conf. (EuroDisplay)*, London, United Kingdom, pp. 54–56 (2013).
39. V. Saveljev and S.-K. Kim, "Three-dimensional moiré display," *J. Soc. Inf. Disp.* **22**(9), 482–486 (2014).
40. H. Liu, A. N. Cartwright, and C. Basaran, "Sensitivity improvement in phase-shifted moiré interferometry using 1-D continuous wavelet transform image processing," *Opt. Eng.* **42**(9), 2646–2652 (2003).
41. A. Martínez, R. Rodríguez-Vera, and J. A. Rayas, "Influence of object roughness on specimen gratings for moiré interferometry," *Opt. Eng.* **40**(9), 1978–1983 (2001).
42. L. Sałbut, K. Patorski, and M. Kujawińska, "Polarization approach to high-sensitivity moiré interferometry," *Opt. Eng.* **31**(3), 434–439 (1992).
43. O. Kafri and I. Glatt, "Moiré deflectometry: a ray deflection approach to optical testing," *Opt. Eng.* **24**(6), 944–960 (1985).
44. W. Chen et al., "Extended dual-grating alignment method for optical projection lithography," *Appl. Opt.* **49**(4), 708–713 (2010).
45. J. Li, H. Shen, and R. Zhu, "Method of alignment error control in free-form surface metrology with the tilted-wave-interferometer," *Opt. Eng.* **55**(4), 044101 (2016).
46. R. D. Hersch and S. Chosson, "Band moiré images," *ACM Trans. Graphics* **23**(3), 239–247 (2004).
47. M. Ragulskis and A. Aleksa, "Image hiding based on timeaveraging moiré," *Opt. Commun.* **282**(14), 2752–2759 (2009).
48. V. Saveljev et al., "About a moiré-less condition for non-square grids," *J. Disp. Technol.* **4**(3), 332–339 (2008).
49. C. Chiang, "Moiré topography," *Appl. Opt.* **14**(1), 177–179 (1975).
50. D. Post, B. Han, and P. Ifju, *High Sensitivity Moiré: Experimental Analysis for Mechanics and Materials*, Springer, New York (1994).
51. M. Ragulskis, A. Aleksa, and L. Saunoriene, "Improved algorithm for image encryption based on stochastic geometric moiré and its application," *Opt. Commun.* **273**(2), 370–378 (2007).
52. I. Amidror, S. Chosson, and R. D. Hersch, "Moiré methods for the protection of documents and products," *J. Phys. Conf. Ser.* **77**, 012001 (2007).
53. V. Ostromoukhov et al., "Anti-counterfeiting features of artistic screening," *Proc. SPIE* **2951**, 126–133 (2010).
54. I. Amidror and R. D. Hersch, "The role of Fourier theory and of modulation in the prediction of visible moiré effects," *J. Mod. Opt.* **56**(9), 1103–1118 (2009).
55. K. Patorski, K. Pokorski, and M. Trusiak, "Fourier domain interpretation of real and pseudo-moiré phenomena," *Opt. Express* **19**(27), 26065–26078 (2011).
56. I. Amidror, *Mastering the Discrete Fourier Transform in One, Two or Several Dimensions*, Springer, London, United Kingdom (2013).
57. V. Saveljev and S.-K. Kim, "Theoretical estimation of moiré effect using spectral trajectories," *Opt. Express* **21**(2), 1693–1712 (2013).
58. V. Saveljev and S.-K. Kim, "Experimental amplitude, period and orientation of the moiré patterns in barrier 3D displays," *J. Inf. Disp.* (2018).
59. V. Saveljev, "Orientations and branches of moiré waves in three-dimensional displays," *J. Korean Phys. Soc.* **57**(6), 1392–1396 (2010).
60. V. Saveljev and S.-K. Kim, "Simulation and measurement of moiré patterns at finite distance," *Opt. Express* **20**(3), 2163–2177 (2012).
61. V. Saveljev, "Moiré effect in cylindrical objects," *J. Korean Phys. Soc.* **68**(9), 1075–1082 (2016).
62. V. Saveljev and J. Kim, "Moiré effect in single-layer cylindrical surface," in *Proc. Optical Society of Korea Winter Annual Meeting*, paper W1A-I-1, Jeongseon, Gangwon, Korea, p. 5 (2017).
63. V. Saveljev and J. Kim, "Towards physical simulation of the moiré effect in nanoparticles," in *Proc. Spring Meeting of Korean Physical Society*, paper A4.03, Daejeon, Korea (2017).
64. G. Strang, *Computational Science and Engineering*, Chapter 4.1, Wellesley-Cambridge University, Wellesley, Massachusetts (2007).
65. C. Huang et al., "Developing the spectral trajectories of major land cover change processes," *Proc. SPIE* **3502**, 155–162 (1998).
66. P. S. Costa-Pereira and P. Maillard, "Estimating the age of cerrado regeneration using Landsat TM data," *Can. J. Remote Sens.* **36**(S2), S243–S256 (2010).
67. V. Saveljev and S.-K. Kim, "Estimation of moiré patterns using spectral trajectories in the complex plane," *Comput. Technol. Appl.* **3**(5), 353–360 (2012).
68. V. Saveljev and S.-K. Kim, "Probability of the moiré effect in barrier and lenticular autostereoscopic 3D displays," *Opt. Express* **23**(20), 25597–25607 (2015).
69. J. Li et al., "Formation mechanism and a universal period formula for the CCD moiré," *Opt. Express* **22**(17), 20914–20923 (2014).
70. K.-B. Kim et al., "Investigation of pattern-induced brightness non-uniformity in active-matrix organic light-emitting diode displays," *Jpn. J. Appl. Phys.* **47**(1), 193–196 (2008).
71. S.-J. Byun et al., "An efficient simulation and analysis method of moiré patterns in display systems," *Opt. Express* **22**(3), 3128–3136 (2014).
72. Y. Zhou et al., "Quantitative measurement and control of optical moiré pattern in an autostereoscopic liquid crystal display system," *Appl. Opt.* **54**(6), 1521–1527 (2015).
73. K. Nagasaki and Y. Bao, "A 3D display with variable depth moiré pattern," in *Proc. SICE Annual Conf.*, pp. 1936–1941 (2008).
74. L. Kong et al., "Parameter design of a parallax barrier based on the color moiré patterns in autostereoscopic display," *Appl. Opt.* **50**(34), H153–H158 (2011).
75. B.-R. Lee et al., "Color moiré simulations in contact-type 3-D displays," *Opt. Express* **23**(11), 14114–14125 (2015).
76. C.-W. Jeon et al., "Wall pattern design to reduce color moiré in autostereoscopic 3D display," *Mol. Cryst. Liq. Cryst.* **613**(1), 63–68 (2015).
77. H. Lee et al., "Fringe periods of color moirés in contact-type 3-D displays," *Opt. Express* **24**(13), 14183–14195 (2016).
78. F. P. Chiang and B. Ranganayakamma, "Deflection measurements using moiré gap effect," *Exp. Mech.* **11**(4), 296–302 (1971).
79. F. P. Chiang and R. M. Juan, "A method to shift moiré fringes using gap effect," *Exp. Mech.* **13**(5), 209–211 (1973).
80. D. Yogev, S. Efrima, and O. Kafri, "Study of the thickness of liquid layers by moiré deflectometry," *Opt. Lett.* **13**(10), 934–936 (1988).
81. J. Kim et al., "Behaviors of moiré fringes induced by plate thickness," *J. Opt.* **17**(3), 1–7 (2015).
82. O. Mikami, "New image-rotation using moiré lenses," *Jpn. J. Appl. Phys.* **14**(7), 1065–1066 (1975).
83. G. Oster and Y. Nishijima, "Moiré patterns," *Sci. Am.* **208**(5), 54–63 (1963).
84. G. Oster, "Optical art," *Appl. Opt.* **4**(11), 1359–1369 (1965).
85. N. J. Wade, "Op art and visual perception," *Perception* **7**(1), 21–46 (1978).
86. R. Parra Toro, *POP ON OP*, Kickstarter (2014), www.parratoro.com.
87. A. Minini, "Andrea Minini, illustrator & graphic designer," andreaminini.myportfolio.com (15 March 2018).
88. P. Dickens, "Pip Dickens, paintings," www.pip-dickens.com (15 March 2018).
89. P. Decrauzat, "Philippe Decrauzat, selected works," www.praz-delavallade.com/philippe-decrauzat (15 March 2018).
90. C. Cruz-Diez, "Carlos Cruz-Diez, Venezuelan, b. 1923," www.artsy.net/artist/carlos-cruz-diez/works (15 March 2018).

Vladimir Saveljev is a research professor at the Myongji University, Yongin, South Korea. He received his PhD from Institute of Automation and Electrometry (IA&E), Siberian Branch of the Russian Academy of Sciences in 2014. After IA&E, he was with Korea Institute of Science and Technology and Hanyang University. He is the author of 150 papers and three book chapters. His current research interests include autostereoscopic 3-D displays, image quality, moiré effect, wavelet transform, and nanoparticles.

Sung-Kyu Kim received his PhD from Quantum Optics Group of Physics, Korea University, in 2000. He spent two years as an invited research scientist at 3-D TV Group of Telecommunications Advancement Organization, Japan. In 2001, he joined at Korea Institute of Science and Technology, where he is currently a principal research scientist. His research interests include optical design of autostereoscopic 3-D display systems, multiview image processing, digital holography, holographic optical elements, and multifocus 3-D display.

Jaisoon Kim received his undergraduate degree in physics education from Seoul National University in 1980, his master's degree in physics education from Seoul National University in 1987, and his doctorate in physics from Korea University in 1999. He has been a research scientist at OSC for 2000–2002 and a professor at Seoul National University for 2002–2009. Currently, he is a professor at the Myongji University, Korea.